CHAPTER 6: THE STRUCTURE OF $Rh(bpy)_2(chrysi)^{3+}$ BOUND TO AN ADENOSINE-ADENOSINE MISMATCH: GENERAL ARCHITECTURE OF THE METALLOINSERTION BINDING MODE[δ]

6.1: INTRODUCTION

Almost fifty years ago, L.S. Lerman proposed four different non-covalent binding modes for small molecules with DNA: (1) electrostatic binding to the sugar phosphate backbone, (2) hydrophobic association with the minor groove, (3) intercalation into the helix by π-stacking between adjacent base pairs, and (4) insertion into the helix by separation and displacement of a base pair.[1] The first three are frequently observed and have been extensively characterized both in solution and in the solid state.[2–6] In contrast, the fourth binding mode, insertion, has eluded researchers almost completely.[7] Recently, however, we have structurally characterized both by crystallography[8] and NMR[9] first examples of insertion into DNA by a small molecule: the mismatch-specific, octahedral metal complex $Rh(bpy)_2(chrysi)^{3+}$ (chrysi = chrysene-5,6-quinone diimine) (**Figure 6.1**).

Because insertion requires the separation of a base pair and the ejection of the bases from the double helix, it follows logically that this binding mode would occur more readily at thermodynamically destabilized sites in DNA. Indeed, to date, insertion has only been definitively observed with octahedral, coordinatively inert metal complexes bearing sterically expansive ligands, such as chrysi or phzi (benzo[a]phenanzine-5,6-quinone diimine)[10]; in both cases, the bulky ligands are 0.5 Å wider than the 10.85 Å

[δ] Adapted from Zeglis, B. M.; Pierre, V. C.; Kaiser, J. R.; Barton, J. K. A bulky rhodium complex bound to an adenosine-adenosine DNA mismatch: general architecture of the metalloinsertion binding mode. *Biochemistry* **2009**, *48(20)*, 4247−4253.

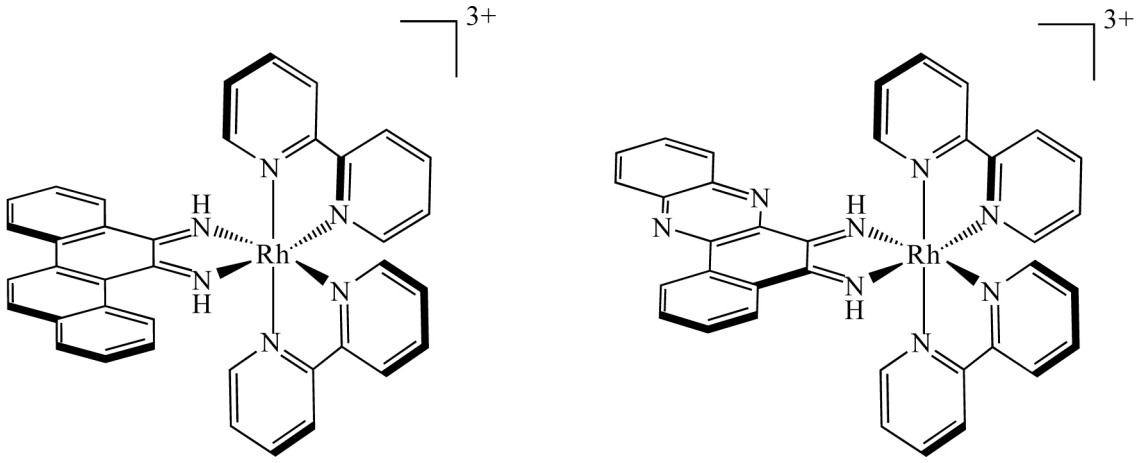

Δ-Rh(bpy)$_2$(chrysi)$^{3+}$ Δ-Rh(bpy)$_2$(phzi)$^{3+}$

Figure 6.1: Structures of Δ-Rh(bpy)$_2$(chrysi)$^{3+}$ and Δ-Rh(bpy)$_2$(phzi)$^{3+}$

span of a matched A•T or G•C base pair. This difference in width precludes the intercalation of the complex at matched sites and thus confers specificity for binding at thermodynamically destabilized mismatched sites.[11]

As we have discussed, rhodium metalloinsertors – most notably $Rh(bpy)_2(chrysi)^{3+}$ and $Rh(bpy)_2(phzi)^{3+}$ – bind single base mismatches with high selectivity and with binding affinities that correlate directly with the local destabilization created by the mismatch.[12–15] Importantly, upon irradiation with UV light, the complexes can photocleave the backbone of a single strand of the mismatched duplex at the binding site. Further still, mismatch binding by this family of complexes is enantiospecific, with only the right-handed, Δ-enantiomer capable of mismatch recognition and binding. Not surprisingly, the remarkable selectivity of these complexes has spurred investigations into their diagnostic and therapeutic applicability. Indeed, in the years since their discovery, metalloinsertors have shown significant promise not only in the detection of single base mismatches[16–18], abasic sites[19, 20], and single nucleotide polymorphisms[21] but also as chemotherapeutic agents.[22–25]

The crystallographic structure of Δ-$Rh(bpy)_2(chrysi)^{3+}$ bound to a palindromic oligonucleotide containing two C•A mismatches has recently been determined (**Figure 6.2**).[8] This structure first revealed that the mismatch-specific rhodium complex does not bind DNA through classical metallointercalation but rather by metalloinsertion: the complex approaches the DNA from the minor groove side and inserts the bulky chrysi ligand at the mismatch site, extruding the mismatched base pairs into the major groove and replacing them in the DNA π-stack. The sugar-phosphate backbone of the DNA opens slightly to accommodate the sterically expansive ligand at the mismatch site.

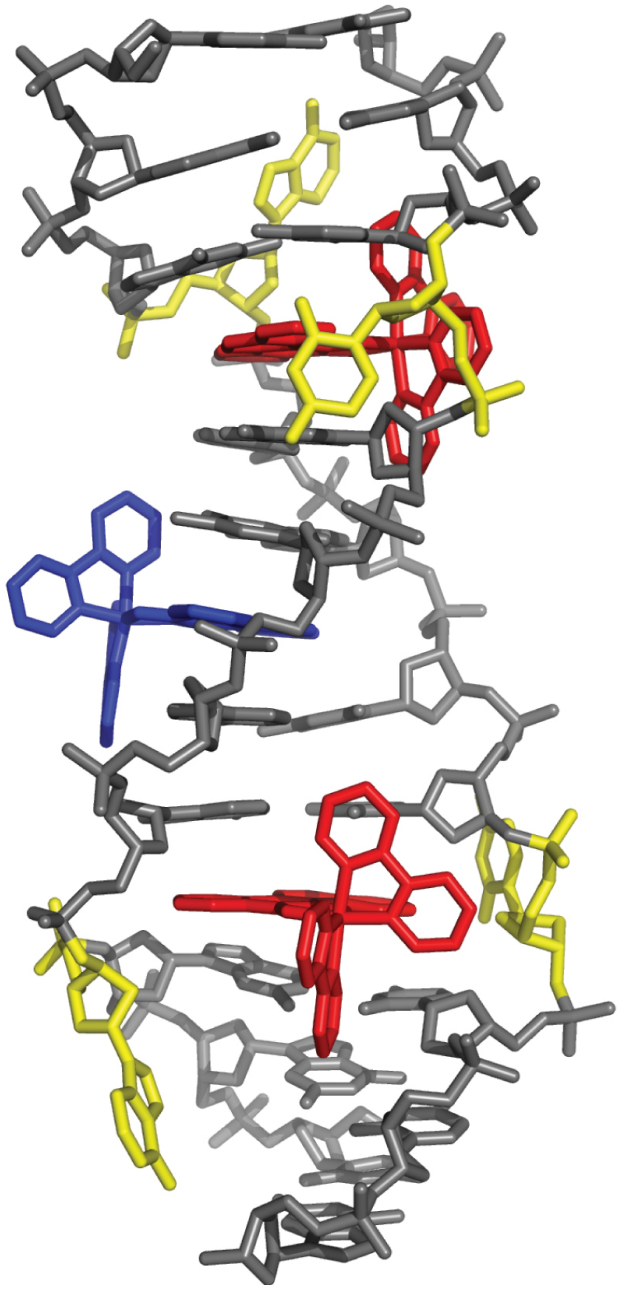

Figure 6.2: Crystal structure of $Rh(bpy)_2(chrysi)^{3+}$ bound to a C•A mismatch.[8] The metal complexes (red) approach the DNA (grey) from the minor groove, ejecting the mismatched bases (yellow) into the major groove and replacing them in the helix. Surprisingly, an intercalated rhodium complex (blue) is also present in the structure.

Overall, the DNA is disturbed very little beyond the insertion site, for all sugars remain in the C2'-endo conformation, and all bases retain an *anti* configuration. Somewhat surprising, however, was the presence of a third rhodium complex in the structure that is bound not through insertion at the mismatched sites but through intercalation at a central 5'-AT-3' step. Given that no detectable binding to a matched site has been observed for these bulky complexes in solution, we considered that this intercalation was the result of crystal packing forces. Subsequent NMR studies of Δ-$Rh(bpy)_2(chrysi)^{3+}$ bound to a similar oligonucleotide containing a C•C mismatch confirmed the insertion binding mode in solution and, significantly, showed no evidence of an intercalated rhodium moiety.[9]

The revelation that these compounds bind mismatches via metalloinsertion rather than metallointercalation provides explanations for two long-standing empirical observations: (1) the correlation between the binding affinity of the metal complex and the thermodynamic destabilization of the mismatched site and (2) the enantiospecificity of the metalloinsertors for the binding and recognition of their target sites. The relationship between binding strength and destabilization stems from the unique base extrusion characteristic of the binding mode: the less stable the mispair, the easier its separation and the more readily the metal complex can bind. The origin of the enantiospecificity lies in the groove-selectivity of metalloinsertion. Unlike metallointercalators, metalloinsertors bind via the narrow and sterically-constrictive minor groove. Simply put, in order to avoid steric clash between the ancillary ligands and the DNA backbone, the right-handed helix can only accommodate the right-handed (Δ) enantiomer.

Yet this structural knowledge can do far more than simply help us explain past observations. A thorough understanding of the detailed structure of metalloinsertion can help us design better recognition agents. However, one structure alone will not suffice. Additional structural information is necessary to shed light on the origin of the intercalated rhodium complex in the first structure and, more importantly, to illustrate the generality of the binding mode.

Here, we describe two crystal structures of Δ-$Rh(bpy)_2(chrysi)^{3+}$ bound to an A•A mismatch. Both structures provide examples of metalloinsertion at a new mismatch, but the two structures differ principally in the presence or absence of a third, intercalated rhodium. The comparison of these structures with studies of the metalloinsertor bound to a C•A and a C•C mismatch illuminates the general architecture of the metalloinsertion binding mode at destabilized sites in DNA.

6.2: EXPERIMENTAL PROTOCOLS

6.2.1: SYNTHESIS AND PURIFICATION

The metalloinsertor Δ-$Rh(bpy)_2(chrysi)^{3+}$ was co-crystallized with a self-complementary oligonucleotide containing two A•A mismatches (5'-$C_1G_2G_3\mathit{A}_4A_5A_6T_7T_8\mathit{A}_9C_{10}C_{11}G_{12}$-3'). The enantiopure rhodium complex was synthesized, purified, and isolated as described previously (see Chapter 2).[16] Standard oligonucleotides were synthesized from phosphoramidites on an ABI 3400 DNA synthesizer and purified both with and without the dimethoxytrityl protecting group via two rounds of reverse-phase HPLC (HP1100 HPLC system with Varian DynaMax™ C18 semi-preparative column, gradient of 5:95 to 45:55 MeCN:50 mM NH_4OAc (aq) over 30

min for DMT-on purification and 2:98 to 17:83 MeCN:50 mM NH_4OAc (aq) over 30 min for DMT-off purification).

6.2.2: CRYSTAL PREPARATION AND DATA COLLECTION

Annealed oligonucleotides were incubated with the rhodium complex before crystallization. Subsequent manipulations were performed with minimal exposure of the complex to light. Two different sets of bright orange crystals, henceforth referred to as **1** and **2**, were obtained, each under a distinct set of conditions. In both cases, thirteen different sequences were screened before crystals were obtained with the sequence described above. Crystal set **1** was grown from a solution of 1 mM double-stranded duplex, 3 mM enantiomerically pure Δ−$Rh(bpy)_2(chrysi)^{3+}$, 20 mM sodium cacodylate (pH 7.0), 6 mM spermine·4HCl, 40 mM NaCl, and 5% 2-methyl-2,4-pentanediol (MPD) equilibrated in sitting drops versus a reservoir of 35% MPD at ambient temperature. The crystals grew in space group $P3_221$ with unit cell dimensions a = b = 48.34 Å, c = 69.50 Å, $\alpha = \beta = 90°$, $\gamma = 120°$, with one biomolecule per asymmetric unit (**Table 6.1**).

Crystal set **2** was grown from a solution of 1 mM double-stranded duplex, 2 mM enantiomerically pure Δ−$Rh(bpy)_2(chrysi)^{3+}$, 20 mM sodium cacodylate (pH 7.0), 6 mM spermine·4HCl, 40 mM KCl, and 5% MPD equilibrated in sitting drop versus a reservoir of 35% MPD at ambient temperature. The crystals grew in space group $P4_32_12$ with unit cell dimensions a = b = 39.02 Å, c = 57.42 Å, $\alpha = \beta = \gamma = 90°$, with half of a biomolecule per asymmetric unit (**Table 6.1**).

	Structure 1	Structure 2
Data Collection		
Space group	$P3_121$	$P4_32_12$
Cell dimensions: a, b, c α, β, γ	 48.3, 48.3, 69.5 90.0, 90.0, 120.0	 39.0, 39.0, 57.4 90.0, 90.0, 90.0
Wavelength	1.0046	1.5418
Resolution	35.0−1.60 (1.69−1.60)	28.71−1.80 (1.90−1.80)
R_{merge}	0.035 (0.499)	0.061 (0.782)
R_{pim}	0.013 (0.288)	0.031 (0.342)
I/σI	26.7 (2.0)	19.1 (2.3)
Completeness, %	99.5 (98.9)	98.7 (97.4)
Redundancy	7.9 (4.2)	6.5 (6.6)
Refinement		
No. of Reflections	22677	4469
R_{work}/R_{free}	0.184/0.227	0.183/0.213
No. of atoms (DNA)	524	262
No. of atoms (RhL_6)	120	90
No. of atoms (water)	89	63
B-factors (DNA)	43.44	25.7
B-factors (complex)	43.44	22.1
B-factors (water)	48.86	41.4
RMS dev. (lengths)	0.013	0.032
RMS dev. (angles)	2.450	4.281

Table 6.1: Data collection and refinement statistics

The data for crystal **1** were collected on beamline 11−1 at the Stanford Synchrotron Radiation Laboratory (Menlo Park, CA; λ = 1.00 Å, 100 K, Marresearch 325 CCD detector). The data for crystal **2** were collected from a flash-cooled crystal at 100 K on an R-axis IV image plate using CuKα radiation produced by a Rigaku (Tokyo, Japan) RU-H3RHB rotating-anode generator with double-focusing mirrors and an Ni filter. Both sets of data were processed with MOSFLM and SCALA from the CCP4 suite of programs.[26]

6.2.3: CRYSTAL STRUCTURE DETERMINATION AND REFINEMENT

Both structures were solved by single anomalous dispersion using the anomalous scattering of rhodium (f" = 3.6 electrons for Rh at λ = 1.54 Å, and f" = 1.7 electrons for Rh at λ = 1.00 Å) with the CCP4 suite of programs. For crystal **1**, 2 heavy atoms were located per asymmetric unit; for crystal **2**, 1.5 heavy atoms were located per asymmetric unit, with one on a special position. Structure **1** was refined with PHENIX v. 1.3 against 1.6 Å data taking into account the anomalous contribution of rhodium; for non-hydrogen atoms, anisotropic temperature factors were refined.[27] The final R_{cryst} and R_{free} were 0.18 and 0.23, respectively. Structure **2** was refined using REFMAC5 v. 5.5.0066 against 1.8 Å data to a final R_{cryst} = 0.18 and R_{free} = 0.21.[a, 28]

In crystal **2**, the rhodium complex located near the crystallographic twofold axis perpendicular to the helical axis of the DNA intercalates in two different orientations linked by symmetry. In crystal **1**, residual density with anomalous contribution was also present near a crystallographic two-fold axis at the end of the duplex, most likely the

[a] The two structures were solved with different but widely employed refinement programs.

result of a disordered cacodylate or chloride ion. In the later stages of refinement for both crystals, riding hydrogens were included. Figures were drawn with Pymol.[29]

6.3: Results and Discussion

6.3.1: Two types of crystals

The palindromic oligonucleotide 5'-$C_1G_2G_3\mathit{A}_4A_5A_6T_7T_8\mathit{A}_9C_{10}C_{11}G_{12}$-3' contains two adenosine-adenosine mismatches, each situated three bases from the end of the strand and separated from one another by a central 5'-AATT-3' tetrad. Here, the duplex was co-crystallized with Δ-$Rh(bpy)_2(chrysi)^{3+}$ for high-resolution x-ray structure determination in order to improve our understanding of metalloinsertion at DNA single base mismatches. Interestingly, diffraction quality crystals with two different space groups ($P3_221$ and $P4_32_12$) were obtained under very similar crystallization conditions. Indeed, both crystals were grown with the same temperature, buffer, pH, type and concentration of precipitant, concentration of DNA, and concentration of spermine. The only differences are the concentration of metalloinsertor and the identity of salt employed: crystal **1** ($P3_221$), containing 2 rhodiums per duplex, was obtained using 3 mM complex and 40 mM NaCl, and crystal **2** ($P4_32_12$), containing 3 rhodiums per duplex, was obtained using 2 mM metalloinsertor and 40 mM KCl. Taken together, the structures of crystal **1** (1.6 Å) and **2** (1.8 Å) provide insights into the structure and generality of metalloinsertion.

6.3.2: STRUCTURE 1

In crystal **1**, the oligonucleotide co-crystallizes with the metalloinsertor in the space group $P3_221$, with six asymmetric units per unit cell. The asymmetric unit contains one DNA duplex complexed with two metalloinsertors (**Figure 6.3**). Significantly, crystallization breaks the C_2 symmetry of the DNA-metalloinsertor palindromic assembly, rendering the two mismatch sites inequivalent and providing two independent views of the mismatched site. Inspection of the unit cell reveals that the duplexes do not stack head-to-tail to form a longer double helix, as is frequently observed with DNA.[3] Instead, it is the inter-duplex π-stacking of the ejected adenosines — either interwoven with the ancillary bipyridine ligand of a nearby rhodium complex or stacked with an adjacent, ejected adenosine — that determines the overall crystal packing and thus the space group (**Figure 6.4**).

At both mismatched sites, the metal complex inserts from the minor groove by separating and ejecting the mismatched bases, and the sterically expansive chrysi ligand of the metalloinsertor replaces the destabilized bases in the helical π-stack (**Figures 6.5** and **6.6**). The two ejected purines are pushed outward into the major groove. One of them remains close and perpendicular to the base stack, while the other folds back to the minor groove in a position stabilized by crystal packing. In both cases, deep insertion in the double helix is not inhibited by the increased steric hindrance of the minor groove; the distance between the rhodium center and the helical axis is 4.8 Å, approximately half the radius of the duplex.

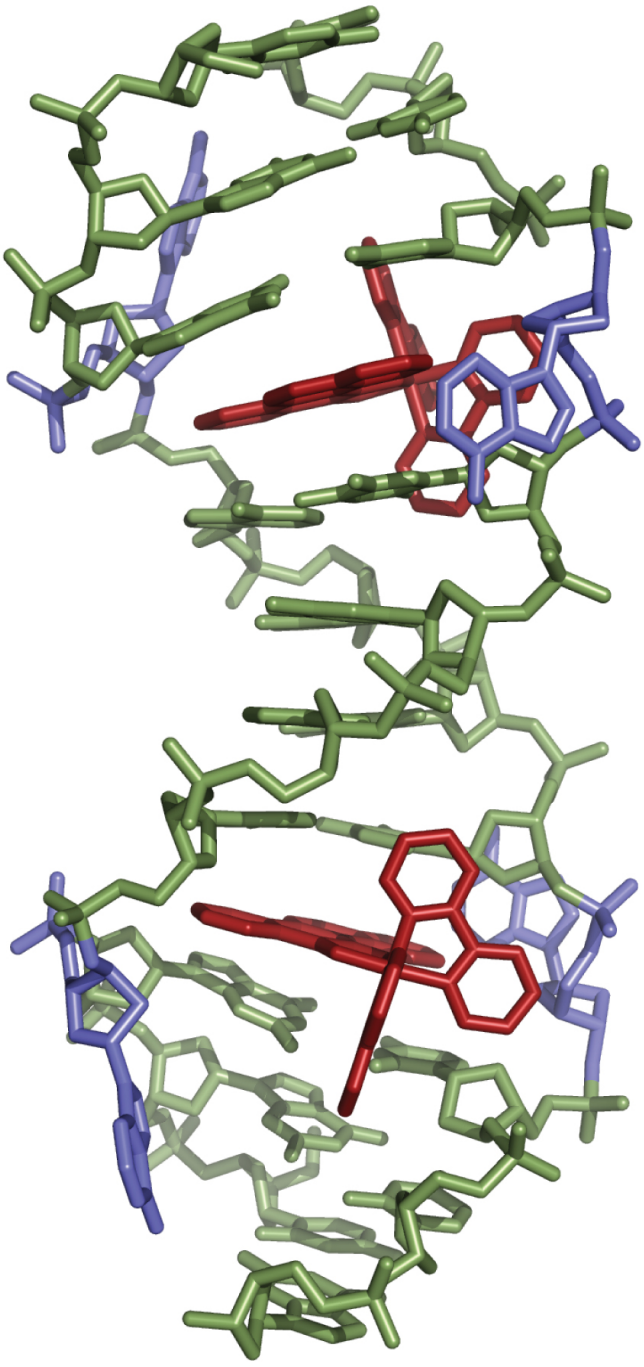

Figure 6.3: Structure 1. Two Δ-Rh(bpy)$_2$(chrysi)$^{3+}$ (red) are inserted, one in each A•A mismatch of the oligonucleotide 5'-CGG*A*AATT*A*CCG-3' (green). The ejected adenosines are shown in blue.

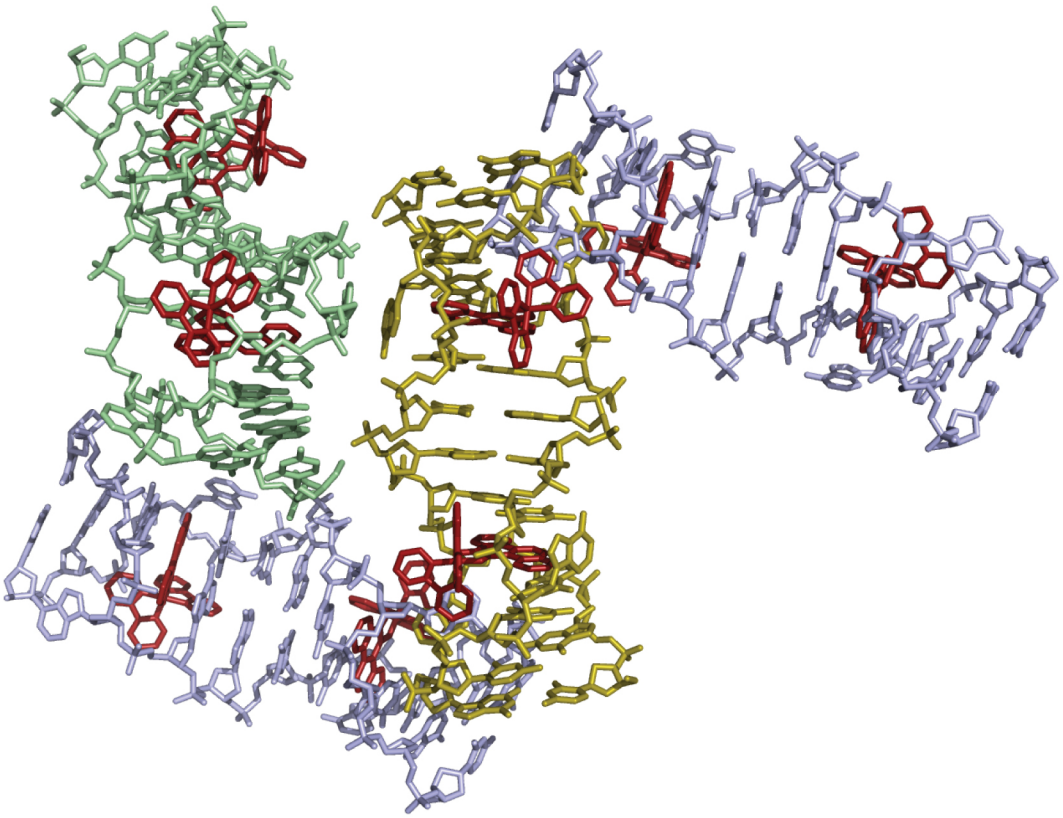

Figure 6.4: Packing of helices in structure 1. The helices are not packed end-to-end, as is commonly observed in crystal structures of DNA oligonucleotides. Instead, inter-duplex π-stacking of the ejected adenosines leads to a packing arrangement that renders the two mismatch sites in a given duplex inequivalent.

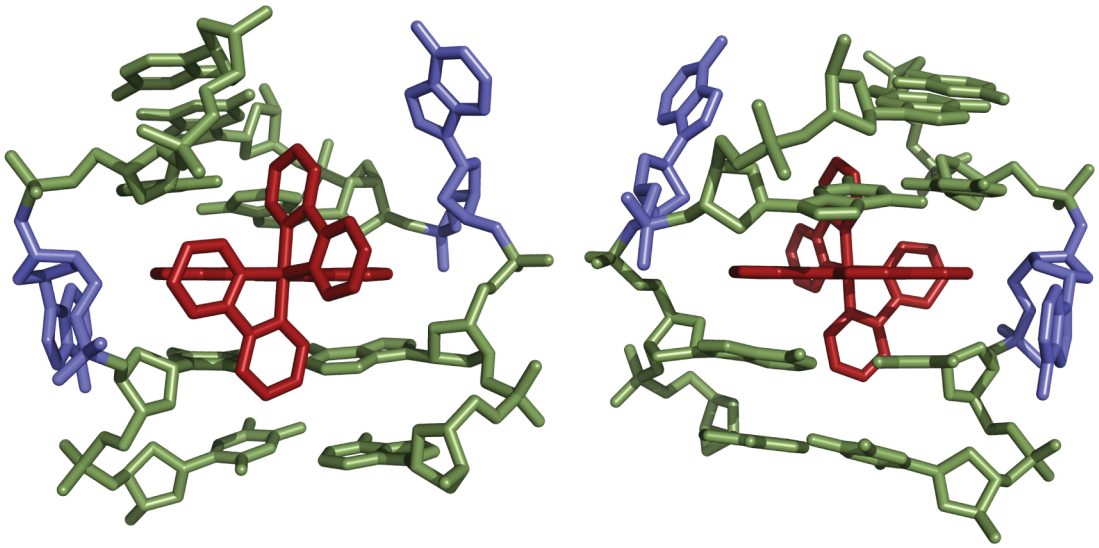

Figure 6.5: Detailed structures of metalloinsertion sites in structure 1. Views of metalloinsertion at an A•A mismatch from the minor (left) and major (right) grooves are shown.

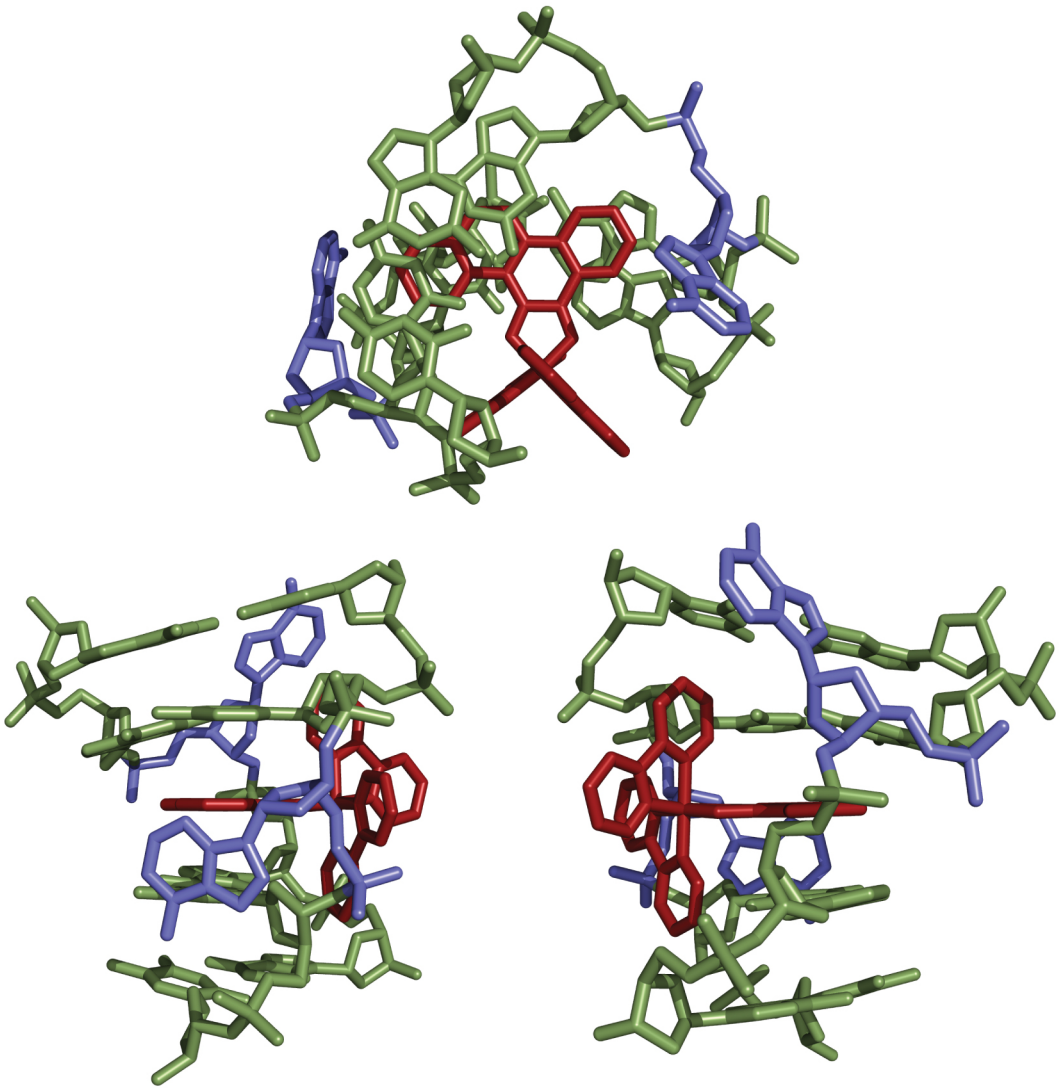

Figure 6.6: Detailed structures of metalloinsertion sites in structure 1. Views of metalloinsertion at an A•A mismatch from along the helical axis (top) and from the phosphate backbone (bottom left, bottom right) are shown.

Upon binding, the rhodium complex inserts deeply to enable complete overlap and stacking with both the purines and pyrimidines of the flanking base pairs. Importantly, these flanking base pairs neither stretch nor shear despite the considerable width of the ligand. All sugars retain their original C_2'-*endo* puckering, and all bases maintain their initial *anti* conformation. To accommodate the inserted rhodium complex, the minor groove at the binding site widens to 19 Å from phosphate to phosphate, between 1 and 1.5 Å wider than other points in the duplex. Aside from the opening of the phosphodiester junctions at the insertion site, however, very little distortion of the DNA is observed (**Tables 6.2** and **6.3**).

The difference between the two insertion sites lies only in the crystal packing of the ejected adenosines. At one of the two insertion sites, one of the ejected adenosines is stacked tightly within the major groove, where it lies perpendicular to the DNA base stack and is not involved in any interduplex interactions or hydrogen-bonding. In contrast, the other adenosine at this site is interwoven with and π-stacks between the ejected adenosine from an adjacent duplex and the ancillary bipyridine ligand of the rhodium complex inserted in that nearby oligonucleotide. At the second insertion site, one of the ejected adenosines again π-stacks between the ejected adenosine from a second adjacent oligonucleotide and the ancillary bipyridine of the rhodium complex intercalated in that nearby DNA. Unlike the first insertion site, however, the other ejected adenosine here does partake in π-stacking, in this case with an extruded adenosine of yet another nearby duplex (**Figure 6.7**).

Base step	Shift (Å)	Slide (Å)	Rise (Å)	Tilt (°)	Roll (°)	Twist (°)
CG/CG	0.8	2.2	3.4	12.0	-1.6	37.6
GG/CC	-0.3	2.7	3.2	-6.1	5.7	34.3
GA/TC	-	-	-	-	-	-
AA/TT	-1.3	1.2	3.3	-4.7	3.8	37.6
AT/AT	0.0	0.1	3.4	1.3	-0.7	29.6
TT/AA	1.3	1.0	3.4	2.2	5.6	36.1
TC/GA	-	-	-	-	-	-
CC/GG	0.4	2.7	3.3	4.7	6.5	34.5
CG/CG	1.0	2.5	3.2	-8.2	2.1	37.3
B-DNA	-0.1	-0.8	3.3	-1.3	-3.6	36

Table 6.2: DNA helical parameters[b] relating consecutive base pairs of structure 1[c]

[b] Geometrical relationships between consecutive base pairs: shift, translation into the groove; slide, translation toward the phosphodiester backbone; rise, translation along the helix axis; tilt, rotation about the pseudo-two-fold axis relating the DNA strands; roll, rotation about a vector between the C1' atoms; and twist, rotation about the helix axis.

[c] Data were calculated by using the program 3DNA.[30]

Base pair	Shear (Å)	Stretch (Å)	Stagger (Å)	Buckle (°)	Propeller (°)	Opening (°)	Pucker
C•G	0.1	-0.1	0.9	-10.0	-2.5	-2.8	C2'-endo
G•C	-0.2	-0.1	-0.0	-0.2	1.1	-3.8	C2'-endo
G•C	-0.4	-0.1	0.6	15.0	-7.2	-1.3	C2'-endo
A•A	-	-	-	-	-	-	C2'-endo
A•T	-0.1	-0.1	0.0	-8.6	7.2	1.5	C2'-endo
A•T	0.1	-0.1	0.1	-0.0	-8.3	3.2	C2'-endo
T•A	-0.0	-0.0	0.0	-0.8	-8.0	1.1	C2'-endo
T•A	-0.1	-0.2	0.1	5.8	9.4	1.7	C2'-endo
A•A	-	-	-	-	-	-	C2'-endo
C•G	0.3	-0.1	0.6	-18.8	-5.8	-0.5	C2'-endo
C•G	0.2	-0.1	0.1	-3.9	2.0	-0.5	C2'-endo
G•C	-0.3	-0.1	0.4	6.2	-5.3	0.7	C2'-endo
B-DNA	0	0.1	0.1	0.1	4.1	-4.1	C2'-endo

Table 6.3: DNA helical parameters for the base pairs of structure 1[d]

[d] Data were calculated by using the program 3DNA.[30]

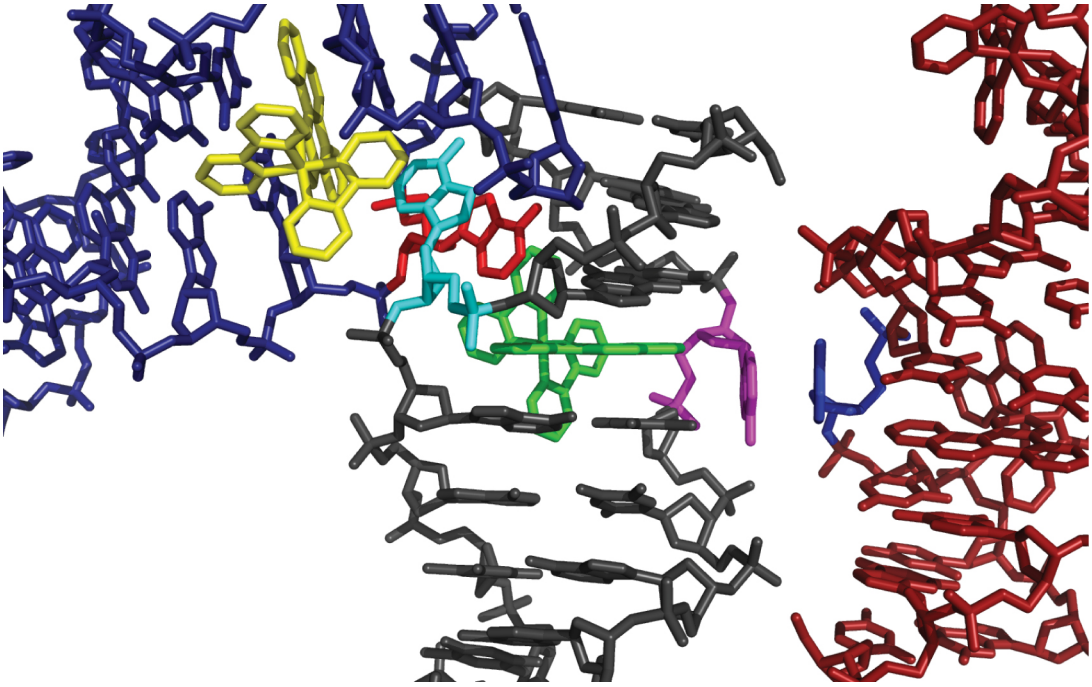

Figure 6.7: Crystal packing by the ejected adenosines at one of the metalloinsertion sites in structure 1. At both insertion sites of the duplex, one ejected adenosine (cyan) π-stacks in an interwoven fashion with the bipyridine ligand of a rhodium complex (yellow) inserted in a nearby crystallographically related oligonucleotide and its corresponding ejected adenosine (red). The bipyridine ligand of the rhodium complex in the original duplex (green) completes the four-component stacking. In only one of the two insertion sites, as shown here, the second mismatched adenosine ejected in the major groove (magenta) π-stacks with a crystallographically equivalent ejected major groove adenosine (blue).

6.3.3: STRUCTURE 2

In crystal **2**, the oligonucleotide co-crystallizes with the metalloinsertor in the space group $P4_32_12$. In this case, the asymmetric unit is a single DNA strand with 1.5 metalloinsertors. Each duplex thus contains three rhodium complexes, one inserted at each of the mismatched sites and a third intercalated between the adenosine and thymine of the central 5'-AT-3' step (**Figure 6.8**). Due to its position on a crystallographic two-fold axis, the central rhodium intercalates in two different orientations. The rhodium complexes at the two mismatched sites are also related by C_2 symmetry, providing a single, independent view of the insertion site (**Figure 6.9**). Interestingly, in all respects other than the identity of the mismatch, this structure is virtually identical to that previously published for Δ-$Rh(bpy)_2(chrysi)^{3+}$ bound to a C•A mismatch.[8]

At the A•A mismatch site, the metalloinsertor approaches the DNA from the minor groove, ejects the mispaired adenines from the helix, and replaces them in the DNA base stack with its own sterically expansive chrysi ligand. Indeed, the metalloinsertor π-stacks with the flanking A•T and C•G base pairs and penetrates so deeply from the minor groove that it is solvent accessible from the major groove. One of the ejected adenosines sits in the major groove, positioned perpendicular to the DNA base stack. The other adenosine bends back into the minor groove, where it π-stacks between the ejected adenosine of an adjacent duplex and a bipyridine ligand of a metalloinsertor bound to that oligonucleotide. Insertion of the rhodium complex into the site is facilitated by a slight widening of the phosphate backbone, from an average of 17.5 Å for well-matched sites to 19 Å for the metalloinsertion sites. Indeed, beyond this

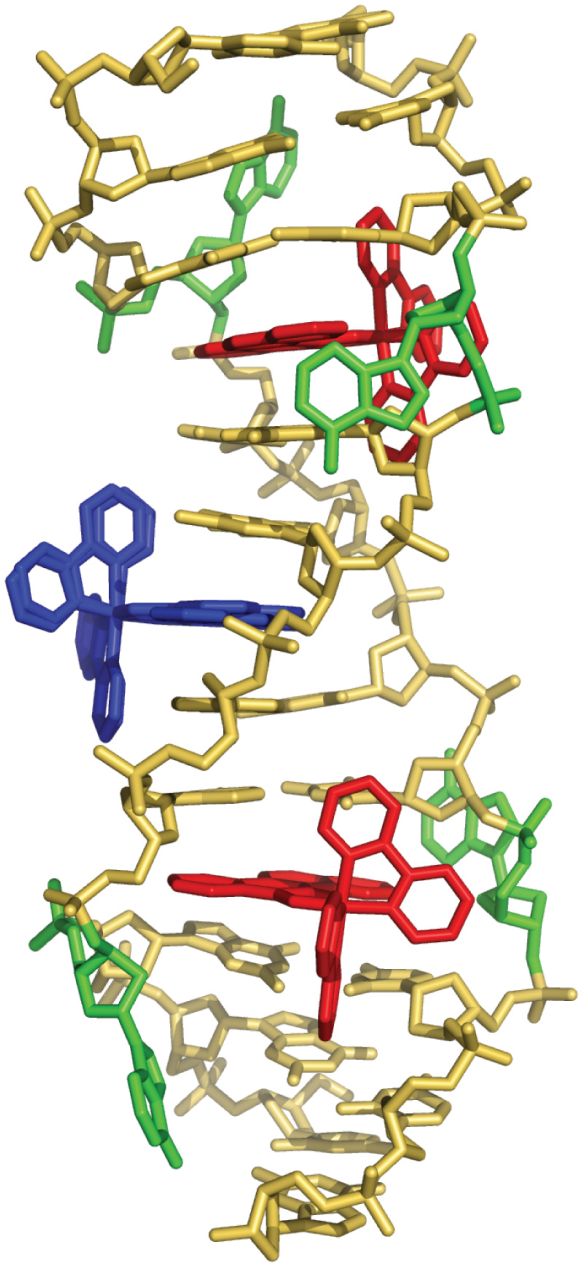

Figure 6.8: Structure 2. Two Δ-Rh(bpy)$_2$(chrysi)$^{3+}$ (red) are inserted, one in each A•A mismatch of the oligonucleotide 5'-CGG*A*AATT*A*CCG-3' (yellow). A third rhodium complex (blue) is intercalated at the central 5'-AT-3' step. The ejected adenosines are shown in green.

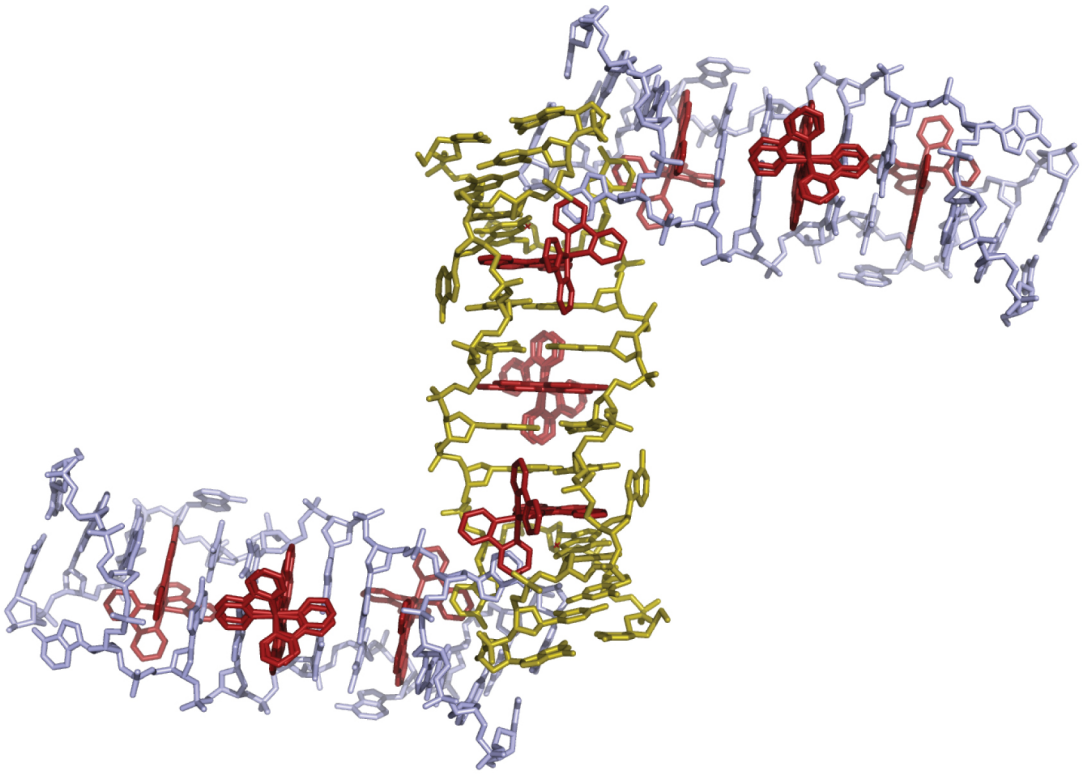

Figure 6.9: Packing of helices in structure 2. The helices are not packed end-to-end, as is commonly observed. Instead, inter-duplex π-stacking of the ejected adenosines leads to packing arrangement in which the two metalloinsertion sites are equivalent.

conformational change, metalloinsertion again distorts the DNA very little. Some buckling of the external flanking C•G base pairs is observed, but all riboses exhibit C2'-*endo* puckering, and all bases retain an *anti* configuration (**Tables 6.4** and **6.5**).

As in the C•A mismatch structure, a third Δ-$Rh(bpy)_2(chrysi)^{3+}$ is also found intercalated at the central 5'-AT-3' step.[8] At this site, the rhodium complex approaches the duplex from the major groove and intercalates the chrysi ligand between adjacent A•T and T•A base pairs, doubling the rise at the intercalation site to 7.1 Å and slightly unwinding the duplex. This binding interaction resembles closely that previously observed in the crystal structure of the sequence-specific metallointercalator Δ-α-$Rh[(R,R)\text{-}Me_2trien](phi)^{3+}$ bound by classical intercalation to its target site.[3] The intercalative binding, like insertion, is accommodated by a slight widening of the phosphate backbone at the intercalation site and is accompanied by some buckling of the adjacent base pairs. Given the exquisite mismatch selectivity of the metalloinsertors in solution, such intercalative binding is a surprise and is almost certainly the result of crystal packing forces. The bipyridines of the intercalated metal complex π-stack with the terminal C•G base pairs of two crystallographically related duplexes, in essence making the intercalated rhodium complex a linchpin for the crystal packing (**Figure 6.10**).

6.3.4: DIFFERENCES BETWEEN THE TWO STRUCTURES

Certainly the most prominent difference between the two structures is the presence or absence of a Δ-$Rh(bpy)_2(chrysi)^{3+}$ intercalated at the central 5'-AT-3' step. Given the similarity in crystallization conditions for crystals **1** and **2**, the rhodium

Base step	Shift (Å)	Slide (Å)	Rise (Å)	Tilt (°)	Roll (°)	Twist (°)
CG/CG	1.1	2.2	3.0	11.0	2.8	40.0
GG/CC	-0.4	2.7	3.3	-6.0	6.1	34.8
GA/TC	-	-	-	-	-	-
AA/TT	-0.8	0.8	3.3	0.4	4.3	32.2
AT/AT	0.0	-0.2	7.1	0.0	-10.4	27.3
TT/AA	0.8	0.8	3.3	-0.4	4.3	32.2
TC/GA	-	-	-	-	-	-
CC/GG	0.4	2.7	3.3	6.0	6.1	34.8
CG/CG	-1.1	2.2	3.0	-11.0	2.8	30.0
B-DNA	-0.1	-0.8	3.3	-1.3	-3.6	36

Table 6.4: DNA helical parameters[e] relating consecutive base pairs of structure 2[f]

[e] Geometrical relationships between consecutive base pairs: shift, translation into the groove; slide, translation toward the phosphodiester backbone; rise, translation along the helix axis; tilt, rotation about the pseudo-two-fold axis relating the DNA strands; roll, rotation about a vector between the C1' atoms; and twist, rotation about the helix axis.

[f] Data were calculated by using the program 3DNA.[30]

Base pair	Shear (Å)	Stretch (Å)	Stagger (Å)	Buckle (°)	Propeller (°)	Opening (°)	Pucker
C•G	0.0	-0.3	0.8	-16.2	-2.4	-4.	C2'-endo
G•C	-0.2	-0.3	0.0	3.4	1.4	-2.1	C2'-endo
G•C	-0.3	-0.1	0.5	18.0	-6.0	0.2	C2'-endo
A•A	-	-	-	-	-	-	C2'-endo
A•T	-0.1	-0.1	0.1	-1.3	8.6	5.0	C2'-endo
A•T	0.1	-0.2	0.2	7.3	-6.9	1.2	C2'-endo
T•A	-0.1	-0.2	0.2	-7.3	-6.9	1.2	C2'-endo
T•A	0.1	-0.1	0.1	-1.3	-8.6	5.0	C2'-endo
A•A	-	-	-	-	-	-	C2'-endo
C•G	0.3	-0.1	0.5	-18.0	-6.0	0.2	C2'-endo
C•G	0.2	-0.3	0.0	-3.4	-1.4	-2.1	C2'-endo
G•C	-0.1	-0.3	0.8	16.2	-2.4	-4.9	C2'-endo
B-DNA	0	0.1	0.1	0.1	4.1	-4.1	C2'-endo

Table 6.5: DNA helical parameters for the base pairs of structure 2[g]

[g] Data were calculated by using the program 3DNA.[30]

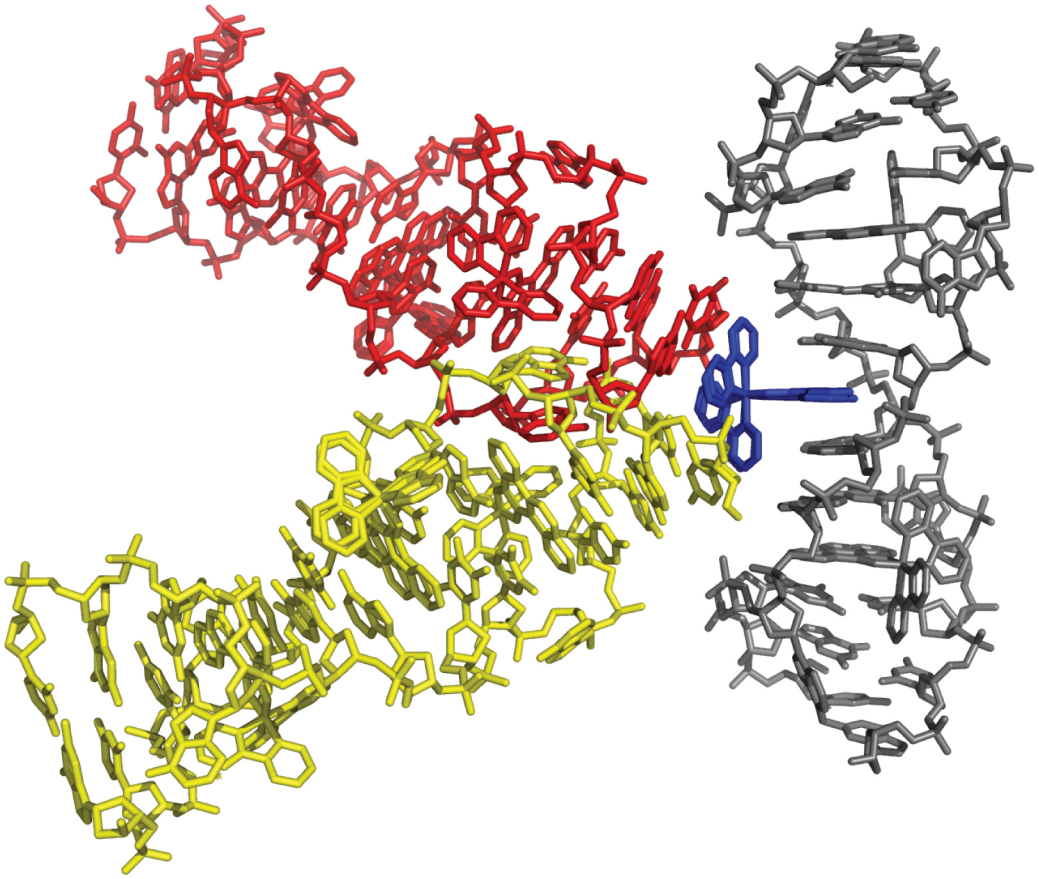

Figure 6.10: Crystal packing of the intercalated $Rh(bpy)_2(chrysi)^{3+}$ in structure 2. Two duplexes (red and yellow) pack against the bipyridine ligands of the intercalated $Rh(bpy)_2(chrysi)^{3+}$ (blue). The metal complex is a linch-pin for the crystal packing.

complex likely has comparable affinity for this central matched site in both cases. That the intercalated rhodium complex *is not* observed in structure **1** therefore strongly substantiates our conclusion that Δ-$Rh(bpy)_2(chrysi)^{3+}$ has negligible affinity for matched DNA and only binds to such sites when intercalation is stabilized by crystal packing-driven π-stacking. In structure **2** and the previously reported C•A mismatch structure, intercalation at the matched site is supported by π-stacking between the ancillary bipyridines of the intercalated rhodium complex and the terminal C•G base pairs of two adjacent helices.[8] Moreover, interwoven stacking between rhodium moieties in these latter duplexes and ejected purines further serves to lock the helices in an orientation that favors intercalative binding. These interactions, taken together, promote the binding of the metalloinsertor in a mode that is not detectable in solution. In fact, the interactions are insufficient to enforce complete intercalation into the double helix (the Rh-helical axis distance in the C•A mismatch structure, for example, is 1.2 Å longer than that of the DNA-bound metallointercalator Δ-α-Rh[(R,R)-Me_2trien](phi)$^{3+}$).[3, 8] These structures thus provide a cautionary example of how crystal packing forces may alter the binding of small molecules to DNA.

The intercalated Δ-$Rh(bpy)_2(chrysi)^{3+}$ in structure **2** is likely also responsible for a second major difference between the structures. Upon superposition of the two structures, it becomes evident that the duplex in structure **1** is slightly bent relative to that in structure **2** (**Figure 6.11**). Examination of the two mismatch-bound chrysi ligands in each structure is particularly instructive in this regard; in structure **2**, the two ligands are nearly coplanar, whereas in structure **1**, they are clearly skew relative to one another (**Figure 6.12)**. Because few perturbations to the duplex are observed beyond the

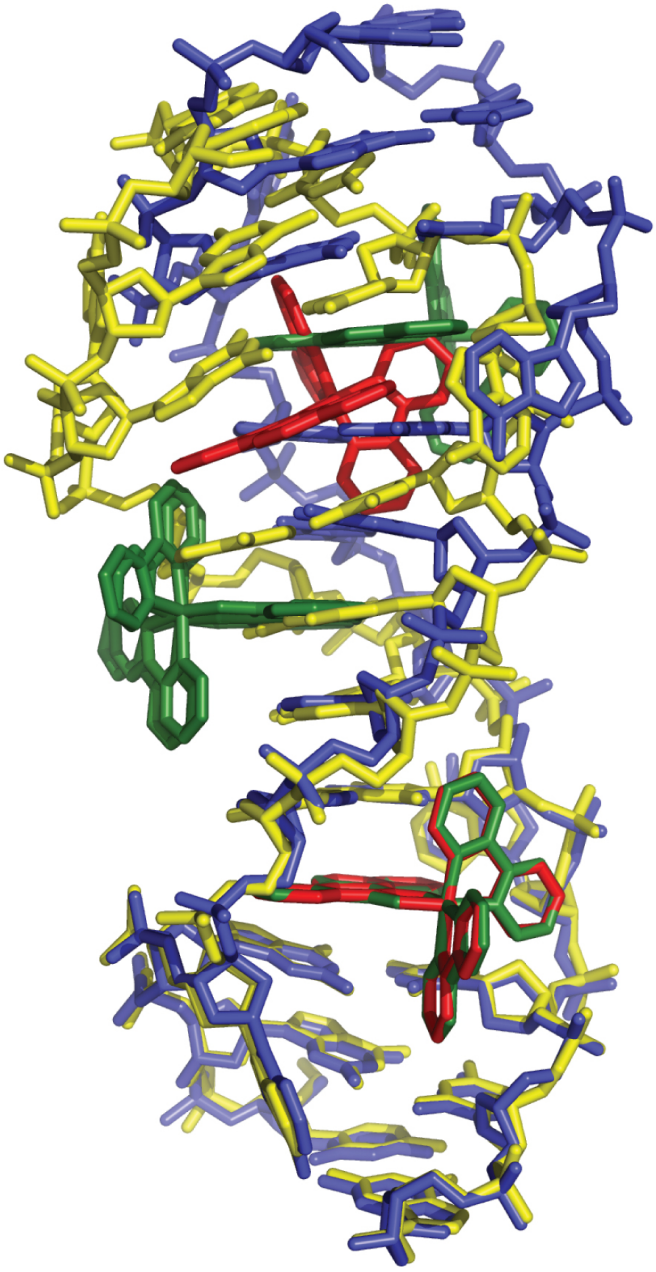

Figure 6.11: Superposition of structures 1 and 2. Structure **1** (yellow DNA with red metal complexes) is contrasted to structure **2** (blue DNA with green metal complexes) by superimposing the bottom, mismatch-bound $Rh(bpy)_2(chrysi)^{3+}$. Note the pronounced bending of the duplex of structure **1**.

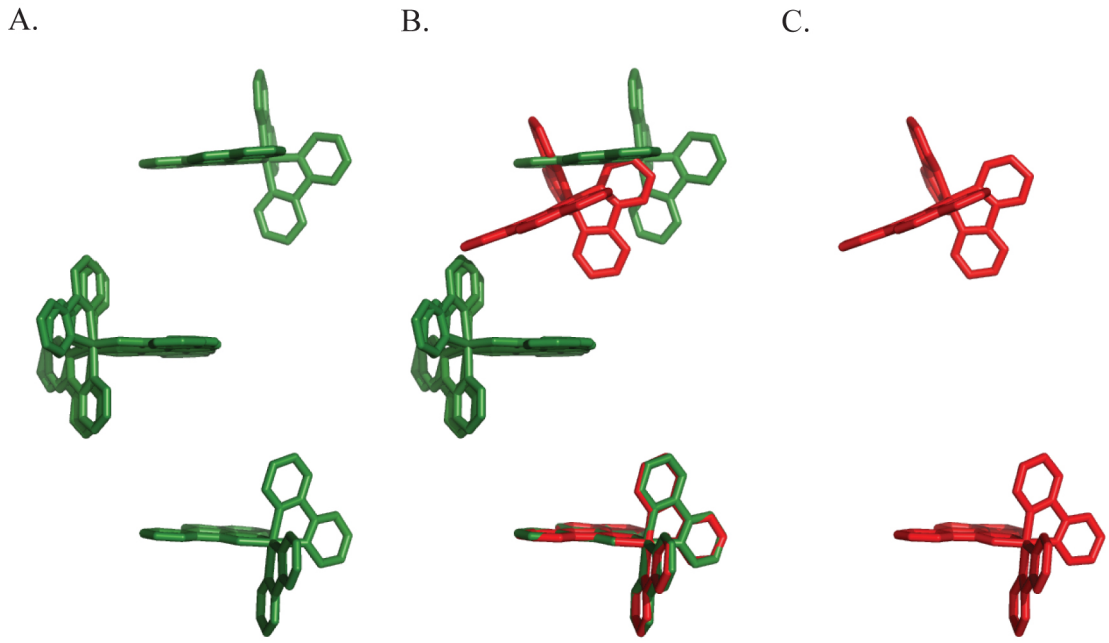

Figure 6.12: The metal complexes of structures 1 and 2. The metal complexes from structure 1 (C) and 2 (A) are shown. A superposition of the two sets of complexes (B) further emphasizes the skewed orientation of those from structure 1 compared to those from structure 2.

mismatched base pair itself in either structure, it is improbable that the metalloinsertors are responsible for this bend in the duplex. Rather, the slight bending is most likely a result of the flexibility associated with the base step. It follows that in structure **2**, the centrally intercalated and well-stacked rhodium complex rigidifies and straightens the helix.

A third major difference between the two structures lies in the stacking of the extrahelical adenosines. The interduplex, four component π-stacking interactions of one of the ejected adenosines at each mismatch site is common to both structures reported here, as well as the previously published C•A mismatch structure.[8] It is with the second ejected base at each mismatch site that differences arise. At each A•A mismatch site in structure **2** and in the C•A mismatch structure, the second ejected adenosine or ejected cytosine, respectively, sits tightly within the major groove, perpendicular to the DNA base stack and uninvolved in any π-stacking or hydrogen bonding. The same is true for the second ejected adenosine at one of the two A•A mismatch sites in structure **1**. At the other A•A site in structure **1**, however, the second ejected adenosine lies near the major groove, remains close to the phosphate backbone, and π-stacks with the ejected adenosine of a nearby duplex (**Figure 6.7**).

6.3.5: GENERAL ARCHITECTURE OF THE INSERTION BINDING MODE

What is perhaps most remarkable about these crystal structures is not their differences but their similarity, not only to one another but also to the earlier structure we obtained.[8] The superposition of the four independent views of Δ-$Rh(bpy)_2(chrysi)^{3+}$ bound to a mismatched site (3 A•A sites, 1 C•A site, **Figure 6.13**) reveals how

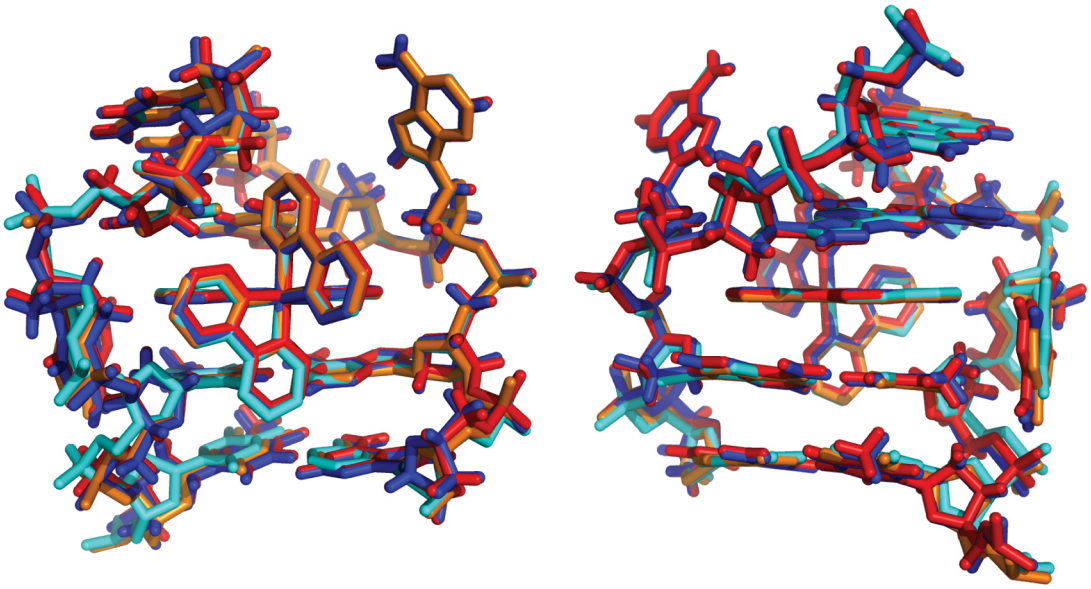

Figure 6.13: General architecture of metalloinsertion. Superposition of the three crystal structures showing insertion of Δ-Rh(bpy)$_2$(chrysi)$^{3+}$ into a single base mismatch viewed looking into the major groove (left) or minor groove (right). The red, blue, and orange structures represent insertion at an A•A mismatch as reported in this work (red and blue are the two sites from structure **1**, and orange is from structure **2**). The cyan structure represents insertion at a C•A mismatch as previously reported.[8]

every detail of the insertion binding mode is maintained regardless of the type of mismatch. In all cases, the DNA conformational changes are localized to the binding site. The metal complex essentially replaces the mismatched base pair; there is no increase in rise, no change in stacking, and no change in sugar puckering. In every case, Δ−$Rh(bpy)_2(chrysi)^{3+}$ is well stacked with the matched DNA bases and penetrates the DNA so deeply that it protrudes from the opposite major groove. Furthermore, in each study, this binding is accommodated by a slight opening in the phosphodiester backbone, and the DNA is only minimally perturbed beyond the insertion site: all bases maintain their original *anti* conformation, all sugars retain a C_2'-*endo* puckering, and flanking base pairs neither stretch nor shear.

Perhaps most remarkable is that the ejected bases, irrespective of their identities, assume nearly identical positions. The ejected bases are not splayed out in random positions, at least not in the structures in the solid state. Instead, their positions seem to be defined, at least in part, by the sugar torsions. In fact, it may be more facile for the bases to be ejected from the minor groove side and accommodated in the major groove; this ejection into the major groove may then be a general characteristic of base pair displacement.[31] Certainly, as evident in **Figure 6.13**, the distinct overlap of these different insertion sites, independent of the identity of the mismatch and crystal packing, must reflect the ease of adopting this type of conformation. These results, all taken together, indicate clearly that insertion into the double helix from the minor groove with ejection of a base pair towards the major groove is a motif that is characteristic of the binding of metal complexes bearing extended ligands to thermodynamically destabilized sites in DNA.

6.4: CONCLUSION

The metalloinsertion of bulky metal complexes at DNA mismatches represents a new paradigm for how small molecules may bind non-covalently to DNA. The structures described here of Δ-$Rh(bpy)_2(chrysi)^{3+}$ bound to thermodynamically destabilized A•A mismatches illustrate the generality of this binding mode. Combined with previous crystallographic and NMR studies on different mismatched oligonucleotides, these structures reveal the architectural characteristics of metalloinsertion: in every case, without regard to the type of mismatch, the metal complex approaches the DNA from the minor groove, ejects the mismatched bases from the helix towards the major groove, replaces the extruded base pair in the π-stack with its own bulky ligand, and perturbs the DNA only minimally beyond the binding site. The similarity in the structures described here along with their clear differences serve furthermore to underscore metalloinsertion as a unique binding interaction, one distinct from intercalation. The presence of an intercalative rhodium in one of the structures also highlights how crystal packing forces can contribute to the solid state structures of small molecules bound non-covalently to DNA. While the information obtained from these structures yields critical and detailed insights, these data must also be considered in context with other data obtained in solution. In future work, it is hoped that these structures will not only prove useful as an illustration of a binding archetype but also in driving the design, synthesis, and application of new generations of small molecules that bind DNA through the insertion mode.

6.5: REFERENCES

1. Lerman, L. S. *Journal of Molecular Biology* **1961,** *3*, 18−30.
2. Neidle, S. *Nucleic Acid Structure and Recognition*. Oxford University Press: 2002.
3. Kielkopf, C. L.; Erkkila, K. E.; Hudson, B. P.; Barton, J. K.; Rees, D. C. *Nature Structural Biology* **2000,** *7* (2), 117−121.
4. Kielkopf, C. L.; White, S.; Szewczyk, J. W.; Turner, J. M.; Baird, E. E.; Dervan, P. B.; Rees, D. C. *Science* **1998,** *282*, 111−115.
5. Bennett, M.; Krah, A.; Wien, F.; Garman, E.; McKenna, R.; Sanderson, M.; Neidle, S. *Proceedings of the National Academy of Sciences U. S. A.* **2000,** *97*, 9476−9481.
6. Coll, M.; Frederick, C. A.; Wang, A. H.; Rich, A. *Proceedings of the National Academy of Sciences U. S. A.* **1987,** *84*, 8385−8389.
7. Lipscomb, L. A.; Zhou, F. X.; Presnell, S. R.; Woo, R. J.; Peek, M. R.; Plaskon, R. R.; Williams, L. D. *Biochemistry* **1996,** *35*, 2818−2823.
8. Pierre, V. C.; Kaiser, J. T.; Barton, J. K. *Proceedings of the National Academy of Sciences U. S. A.* **2007,** *103*, 429−434.
9. Cordier, C.; Pierre, V. C.; Barton, J. K. *Journal of the American Chemical Society* **2007,** *129*, 12287−12295.
10. Junicke, H.; Hart, J. R.; Kisko, J. L.; Glebov, O.; Kirsch, I. R.; Barton, J. K. *Proceedings of the National Academy of Sciences U. S. A.* **2003,** *100*, 3737−3742.
11. Zeglis, B. M.; Pierre, V. C.; Barton, J. K. *Chemical Communications* **2007**, 4565−4579.
12. Jackson, B. A.; Alekseyev, V. Y.; Barton, J. K. *Biochemistry* **1999,** *38* (15), 4655−4662.

13. Jackson, B. A.; Barton, J. K. *Journal of the American Chemical Society* **1997,** *119* (52), 12986−12987.

14. Jackson, B. A.; Barton, J. K. *Biochemistry* **2000,** *39* (20), 6176−6182.

15. Jackson, B. A.; Henling, L. M.; Barton, J. K. *Inorganic Chemistry* **1999,** *38* (26), 6218−6224.

16. Zeglis, B. M.; Barton, J. K. *Nature Protocols* **2007,** *2* (2), 357−371.

17. Zeglis, B. M.; Barton, J. K. *Journal of the American Chemical Society* **2006,** *128* (17), 5654−5655.

18. Lim, M. H.; Lau, I. H.; Barton, J. K. *Inorganic Chemistry* **2007,** *46*, 9528−9530.

19. Zeglis, B. M.; Boland, J. A.; Barton, J. K. *Journal of the American Chemical Society* **2008,** *130* (24), 7530−7531.

20. Zeglis, B. M.; Boland, J. A.; Barton, J. K. *Biochemistry* **2009,** *48* (5), 839−849.

21. Hart, J. R.; Johnson, M. D.; Barton, J. K. *Proceedings of the National Academy of Sciences of the United States of America* **2004,** *101* (39), 14040−14044.

22. Petitjean, A.; Barton, J. K. *Journal of the American Chemical Society* **2004,** *126* (45), 14728−14729.

23. Schatzschneider, U.; Barton, J. K. *Journal of the American Chemical Society* **2004,** *126* (28), 8630−8631.

24. Ernst, R. J.; Song, H.; Barton, J. K. *Journal of the American Chemical Society* **2009,** *131* (6), 2359−2366.

25. Hart, J. R.; Glebov, O.; Ernst, R. J.; Kirsch, I. R.; Barton, J. K. *Proceedings of the National Academy of Sciences U. S. A.* **2006,** *103*, 15359−15363.

26. Collaborative Computational Project Number 4. *Acta Crystallographica* **1994,** *D50*, 760−763.

27. Adams, P. D.; Grosse−Kunstleve, R. W.; Hung, L. W.; Ioerger, T. R.; McCoy, A. J.; Moriarty, N. W.; Read, R. J.; Sacchettini, J. C.; Sauter, N. K.; Terwilliger, R. C. *Acta Crystallographica* **2002,** *D58*, 1948−1954.

28. Murshudov, G. N.; Vagin, A. A.; Dodson, E. J. *Acta Crystallographica* **1997,** *D53*, 240−255.

29. DeLano, W. L. *The PyMOL Molecular Graphics System*, DeLano Scientific: San Carlos, CA, 2002.

30. Lu, X. J.; Olson, W. K. *Nucleic Acids Research* **2003,** *31*, 5108−5121.

31. Peng, T.; Dohno, C.; Nakatani, K. *Angewandte Chemie−International Edition* **2006,** *45*, 5623−5626.